

Model of thermal buoyancy in cavity-ventilated roof constructions

Journal of Building Physics

1–19

© The Author(s) 2021

Article reuse guidelines:

sagepub.com/journals-permissions

DOI: 10.1177/1744259120984189

journals.sagepub.com/home/jen

Toivo Säwén¹ , Martina Stockhaus¹, Carl-Eric Hagentoft¹, Nora Schjøth Bunkholt² and Paula Wahlgren¹

Abstract

Timber roof constructions are commonly ventilated through an air cavity beneath the roof sheathing in order to remove heat and moisture from the construction. The driving forces for this ventilation are wind pressure and thermal buoyancy. The wind driven ventilation has been studied extensively, while models for predicting buoyant flow are less developed. In the present study, a novel analytical model is presented to predict the air flow caused by thermal buoyancy in a ventilated roof construction. The model provides means to calculate the cavity Rayleigh number for the roof construction, which is then correlated with the air flow rate. The model predictions are compared to the results of an experimental and a numerical study examining the effect of different cavity designs and inclinations on the air flow rate in a ventilated roof subjected to varying heat loads. Over 80 different test set-ups, the analytical model was found to replicate both experimental and numerical results within an acceptable margin. The effect of an increased total roof height, air cavity height and solar heat load for a given construction is an increased air flow rate through the air cavity. On average, the analytical model predicts a 3% higher air flow rate than found in the numerical study, and a 20% lower air flow rate than found in the experimental study, for comparable test set-ups. The model provided can be used to predict the air flow rate in cavities of varying design, and to quantify the impact of suggested roof design changes. The result can be used as a basis for estimating the moisture safety of a roof construction.

¹Department of Architecture and Civil Engineering, Chalmers University of Technology, Gothenburg, Sweden

²SINTEF Community, Department of Architecture, Materials and Structures, Trondheim, Norway

Corresponding author:

Toivo Säwén, Department of Architecture and Civil Engineering, Chalmers University of Technology, Sven Hultins Gata 6, Gothenburg, SE-412 96, Sweden.

Email: sawen@chalmers.se

Keywords

Air flow, building envelope, roof construction, analytical model, cavity ventilation

Introduction

The purpose of a roof is to act as a climate shelter to maintain a good indoor climate in a building. As it is a part of the building envelope, it is exposed to varying weather conditions. To protect the construction and ensure the roof function, heat and moisture must either be prevented from entering the construction, or be removed (Gullbrekken, 2018). A common way of achieving this in the Nordic building tradition is with a ventilated air space as one of the layers in the construction, referred to as the air cavity. The air cavity is typically located between the outer rain protective layer and the thermal insulation, as seen in Figure 1. In the roof, the ventilation of this cavity is typically driven by natural effects, that is wind and thermal buoyancy caused by temperature gradients (Hagentoft, 2001).

The climate in the Nordic region ranges from humid continental to subarctic, with warm to mild summers and cold winters (SMHI, 2019). The traditional use for cavity ventilation was to remove heat transmitted through the insulating layer of a roof (Blom, 1991). This reduces roof surface temperatures in order to avoid snow melting and reforming as icicles at the eaves. As demands on building envelope energy efficiency have increased in recent decades, snow melting is less pertinent as

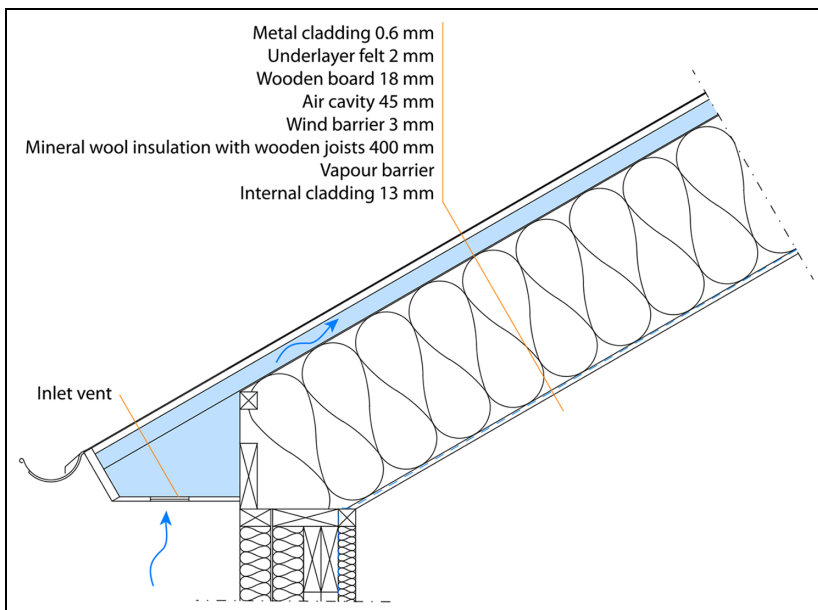


Figure 1. Reference construction used in case study, typical for the Nordic building tradition.

improved insulation causes a smaller heat transmission through the roof. However, the reduced temperatures cause a larger risk for moisture problems. Consequently, moisture removal is the main purpose for air cavity ventilation in current roof constructions (Blom, 2001; Petersson, 2009).

To predict the efficiency of a ventilated construction, a building performance engineer must be able to predict the air flow rate and thermal conditions in the air cavity. Air cavities in walls have been studied experimentally (Falk, 2014), and numerically (Nore et al., 2010; Van Belleghem et al., 2015). The research on roof air cavities is more limited. Studies have been performed on the air flow rate in air cavities considering wind as a driving force (Gullbrekken, 2018). Thermal buoyancy has also been studied, but mostly from the perspective of heat removal in hotter climates (Biwolé et al., 2008; Bunnag et al., 2004; Chami and Zoughaib, 2010; DeWith et al., 2009; Lee et al., 2009; Li et al., 2016; Manca et al., 2014; Susanti et al., 2008). An experimental study on the ventilation of wall air cavities from a moisture perspective was performed by Vanpachtenbeke et al. (2017). An experimental study on moisture levels in ventilated roof cavities was performed by Viljanen et al. (2020).

Some analytical models of the hygrothermal behaviour of roof air cavities have previously been proposed. Such models, including the modelling of air flow resistance, are described in Liersch (1986) and Hagentoft (1991). Blom (2001) describes the development of a model for predicting thermal conditions, as well as a comparative field study, with the main focus on snow melting. An analytical model for air cavity air flow is provided in Griffith (2006), however with more focus on the detailed modelling of the thermal conditions rather than the air flow conditions. A statistical model for estimating the climatic conditions in the air cavity based on internal and external climate was developed by Tieben et al. (2020).

To be able to provide robust solutions even when considering current design trends such as longer, highly insulated roofs and novel eaves design solutions, a means of modelling the air flow in a wide range of design options is required. To the knowledge of the authors, there are currently no detailed and validated yet flexible and efficient calculation models readily available for the design of the air cavity in ventilated roof constructions. This leaves only experience and in some cases standardised local regulations (an overview is provided by Gullbrekken, 2018), or alternatively resource-consuming numerical models, as a basis for the roof design.

The aim of the present study is to provide a flexible and efficient analytical model for characterising a roof construction with regards to the potential for buoyant air flow, especially relevant in colder Nordic climates where moisture removal is the main purpose of air cavity ventilation. Only the effect of thermal buoyancy is studied, the interaction with wind driven flow considered out of scope.

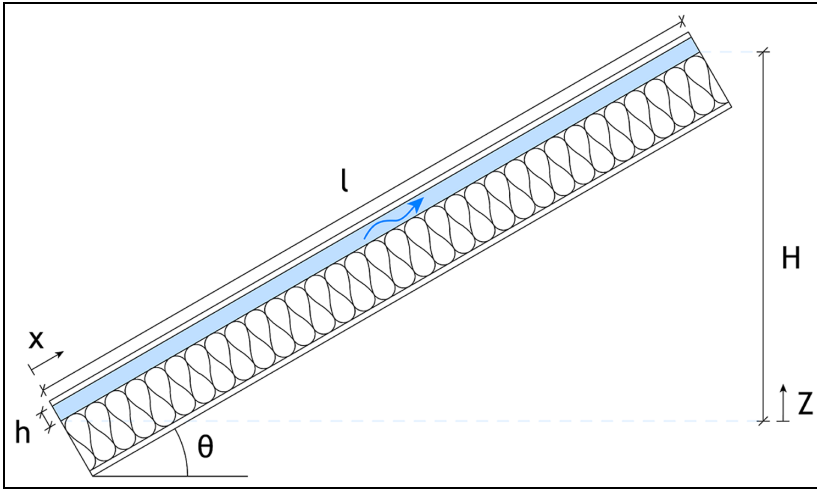


Figure 2. Schematic representation of a cavity ventilated roof construction. Upper case symbols refer to the global coordinate system, while lower case symbols refer to the local coordinates of the cavity. Here, h [m] is the cavity height, l [m] is the cavity length, θ [°] is the roof inclination and H [m] is the total roof height. The coordinate x is parallel to the air cavity, while the coordinate Z is in the direction of gravity.

Thermal Buoyancy Model

This section describes the theoretical background of the analytical model developed in this study, henceforth referred to as the Thermal Buoyancy Model. A schematic drawing of a cavity ventilated roof construction is provided in Figure 2. The air flow rate through a section of the cavity of width 1 m, \dot{V} [m³/s·m], is related to the velocity of the flowing air and the geometry of the cavity through equation (1):

$$\dot{V} = u_m \cdot h \quad (1)$$

where u_m [m/s] is the mean air velocity, and h [m] is the cavity height.

Thermal buoyancy is the effect of temperature gradients causing density differences in a fluid, which generates a pressure difference leading to a flow. The temperature gradient is caused by cool air entering the air cavity at the inlet, and then being heated by the sun-heated external roof surface as it flows, according to equation (2) (Arfvidsson et al., 2017). A temperature gradient may also be caused by under-cooling of the external roof surface, for example by night-time long-wave radiation, when air may be cooled upon entering the cavity and flow downward. However, this case is not directly treated in this study.

$$T_a(x) = T_0 - (T_0 - T_e) \cdot e^{\frac{-x}{l_0}} \quad (2)$$

where T_a [K] is the air temperature along the cavity length, T_0 [K] is the effective air temperature of the cavity, T_e [K] is the temperature of the outdoor air entering the cavity, x [m] is the distance from the inlet as defined in Figure 2 and l_0 [m] is the characteristic length of the cavity. The characteristic length is a measure for the thermal disturbance of the air, calculated according to equation (3):

$$l_0 = \rho \cdot c_p \cdot \dot{V} \cdot \alpha_0^{-1} \quad (3)$$

where ρ [kg/m³] is the density of the air entering the cavity, c_p [J/kg · K] is the specific heat capacity of air at constant atmospheric pressure, h [m] is the cavity height, u_m [m/s] is the mean air velocity in the cavity and α_0 [W/(m² · K)] is the effective heat transfer coefficient of the cavity.

The parameters T_0 and α_0 depend on the thermal properties of the materials in the roof, and the thermal conditions of the system. For steady-state conditions, these parameters can be calculated through the definition of the thermal network of the roof construction, which is then reduced according to Figure 3 (Hagentoft, 2001).

The thermal network displayed in Figure 3 considers heat transmission from the indoor and outdoor air, radiative heating of the roof surface by solar radiation, heat losses caused by longwave radiation, as well as convective and radiative heat transfer within the air cavity. Such a thermal network may be expanded to the desired complexity, and reduced according to techniques described by Hagentoft (2001). The reduction of the network in Figure 3 is detailed in Svantesson and Sävén (2019).

The pressure difference caused by this temperature gradient can be described through equation (4) (Hansen et al., 1992):

$$\Delta P_S = g \cdot \int_0^H \rho - \rho_{cavity}(Z) dZ \quad (4a)$$

$$\Delta P_S = g \cdot \beta \cdot \rho \cdot \sin \theta \cdot (T_0 - T_e) \cdot \int_0^l 1 - e^{-\frac{x}{l_0}} dx \quad (4b)$$

where ΔP_S [Pa] is the stack effect pressure difference over the air cavity. With the air being heated along the cavity length, the temperature gradient is positive, causing the air to be pushed upward. Further, g [m/s²] is the gravitational constant, x and Z [m] are defined according to Figure 2, β [K⁻¹] is the coefficient of thermal expansion, θ [°] is the roof inclination and ρ [kg/m³] is the outdoor air density. The density gradient $\rho_{cavity}(Z)$ is converted to a temperature gradient using equations (2) and (3), and the Boussinesq approximation that all fluid properties besides density remain constant with respect to temperature.

While the thermal conditions govern the driving force for air flow, the geometric conditions cause a flow resistance S [Pa/(m³/s)]. This is caused partly by frictional pressure losses S_f as the air flows along the air cavity, and partly by local losses S_ξ

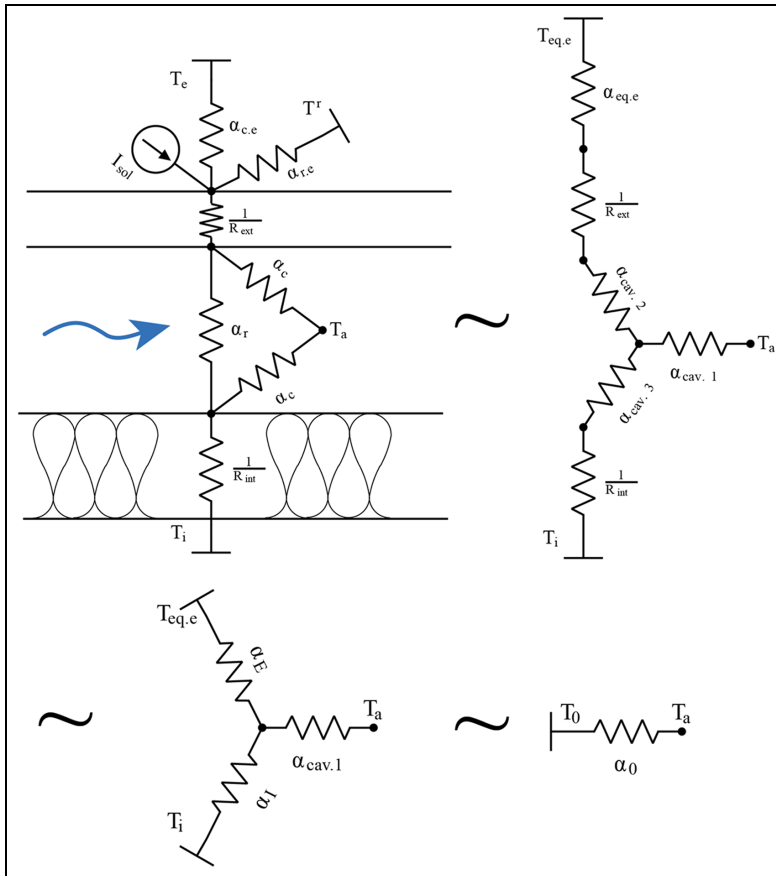


Figure 3. Thermal network of the cavity, reduced according to Hagentoft (2001). In the first step, T_a [K] is the cavity air temperature, T_e [K] is the outdoor air temperature, T_i [K] is the indoor air temperature, T^r [K] is the sky temperature, α_c [$\text{W}/(\text{m}^2 \cdot \text{K})$] refers to convective heat transfer coefficients, α_r [$\text{W}/(\text{m}^2 \cdot \text{K})$] refers to radiative heat transfer coefficients, R [$\text{m}^2 \cdot \text{K}/\text{W}$] refers to heat transfer resistances of the surrounding materials, and I_{sol} [W/m^2] refers to the portion of the solar heat load absorbed by the roof surface. In the second and third steps, equivalent fictive heat transfer coefficients α_{cav} , α_E and α_I [$\text{W}/(\text{m}^2 \cdot \text{K})$] have respectively been defined in the $\Delta \rightarrow Y$ network transformation. Finally in the fourth step, all of the external influences on the cavity air temperature can be described through T_0 [K] and α_0 [$\text{W}/(\text{m}^2 \cdot \text{K})$]. The full derivation of this thermal network is provided in Svantesson and Säwén (2019).

caused by air contraction and expansion at the inlet and outlet of the cavity (Kronvall, 1980), as well as local obstructions to air flow. Assuming laminar flow conditions, the total air flow resistance can be calculated according to

$$S = S_f + S_\xi \quad (5)$$

The frictional flow resistance is independent of the air flow rate. Based on Poiseuille's law, it can be calculated as follows (Kronvall, 1980):

$$S_f = \frac{32 \cdot \mu \cdot l}{\phi \cdot D_h^2 \cdot b \cdot h} \quad (6a)$$

$$\phi = \frac{2}{3} + \frac{11}{24} \cdot \frac{h}{b} \cdot \left(2 - \frac{h}{b}\right) \quad (6b)$$

$$D_h = \frac{2 \cdot b \cdot h}{h + b} \quad (6c)$$

where μ [Pa·s] is the dynamic viscosity of air, b [m] is the cavity width, h [m] is the cavity height, ϕ is a non-dimensional geometric factor, and D_h [m] is the hydraulic diameter of the cavity.

The influence of local losses, however, is air flow rate dependent. The Reynolds number, Re , can be defined to represent the air flow rate non-dimensionally:

$$Re = \rho \cdot \frac{u_m \cdot D_h}{\mu} \quad (7)$$

where u_m [m/s] is the mean velocity of the flowing fluid. For a simplified case with no obstruction at the air inlets and outlets, the air flow resistance due to local losses can then be described through the following formula (Kronvall, 1980):

$$S_\xi = \mu \cdot \frac{Re}{(b + h) \cdot D_h^2} \cdot (1 + K_c(Re)) \quad (8a)$$

$$K_c(Re) = \begin{cases} 0.98 \cdot Re^{-0.03} & \text{if } Re < 1000 \\ 10.59 \cdot Re^{-0.374} & \text{if } 1000 < Re < 2000 \end{cases} \quad (8b)$$

where K_c is an empirically determined factor. For a given roof construction, the air flow resistance due to local losses may instead be calculated based on given pressure loss data, for example, for a fire-resistant air vent or a similar inlet design.

The result of the above equations can be summarised through equation (9), which defines the air flow rate as a function of the pressure difference and air flow resistance:

$$\dot{V} = \frac{\Delta P_S}{S} \quad (9)$$

However, considering equation (4), we find that ΔP_S is a function of both $(T_0 - T_e)$ and l_0 , and by extension of \dot{V} . Equations (5) and (8) provide that S is a function of \dot{V} . Summarising this, we can define the function f as shown in equation (10):

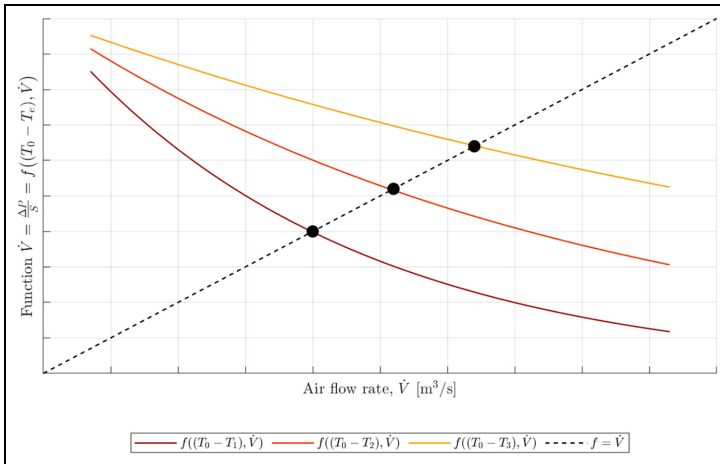


Figure 4. Schematic representation of the relationship in equation (10). Here, T_0 [°C] is constant and T_1 , T_2 and T_3 [°C] refer to different outdoor air temperatures.

$$f((T_0 - T_e), \dot{V}) = \frac{\Delta P_s((T_0 - T_e), \dot{V})}{S(\dot{V})} \quad (10)$$

As schematically shown in Figure 4, the function f will have a different behaviour for any given driving temperature difference ($T_0 - T_e$). By producing such curves for each ($T_0 - T_e$), we are able to predict the air flow rate by locating the point $f((T_0 - T_e), \dot{V}) = \dot{V}$. This is the principal task performed by the Thermal Buoyancy Model, the inner workings of which are further described in the following.

As equation (9) is dependent on the geometric and thermal conditions of the air cavity, a non-dimensional representation of these conditions allows a direct prediction of the air flow rate for any given construction. The air flow conditions caused by thermal buoyancy can be represented by the cavity Rayleigh number Ra_c , defined as (Hagentoft, 1991):

$$Ra_c = \frac{\rho \cdot c_p \cdot g \cdot \beta \cdot \rho \cdot H \cdot (T_0 - T_e)}{\alpha_0} \quad (11)$$

The first factor, referred to as the cavity Prandtl number Pr_c , is dependent on the material properties of the construction and the air, while the second factor, called the cavity Grashof number Gr_c , describes the driving forces and flow resistances.

Inserting equation (4a) into equation (9) and solving the integral provides the following:

$$\dot{V} = \frac{g\beta\rho H(T_0 - T_e)}{S} \cdot \left(1 - \frac{l_0}{l} + \frac{l_0}{l} e^{-\frac{l}{l_0}}\right) \quad (12)$$

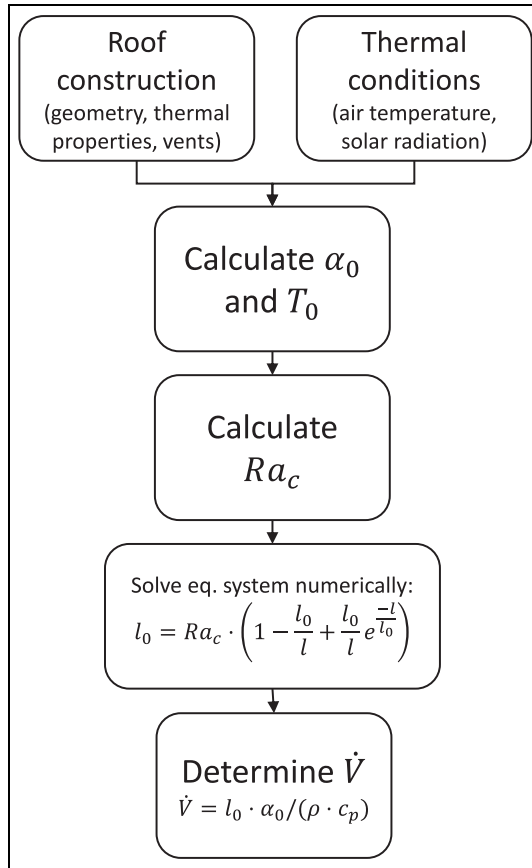


Figure 5. Calculation method of the Thermal Buoyancy Model (TBM).

which when combined with equations (3) and (11) provides

$$l_0 = \frac{\rho \cdot c_p}{\alpha_0} \cdot \dot{V} = Ra_c \cdot \left(1 - \frac{l_0}{l} + \frac{l_0}{l} e^{-\frac{l}{l_0}}\right) \quad (13)$$

Solving this equation system yields a solution for l_0 which in turn provides the resulting thermal conditions and air flow rate. In the Thermal Buoyancy Model, the equation system is solved using the numerical *vpasolve* function provided by the Symbolic Math Toolbox (MATLAB, 2020). The full solution sequence is provided in Figure 5.

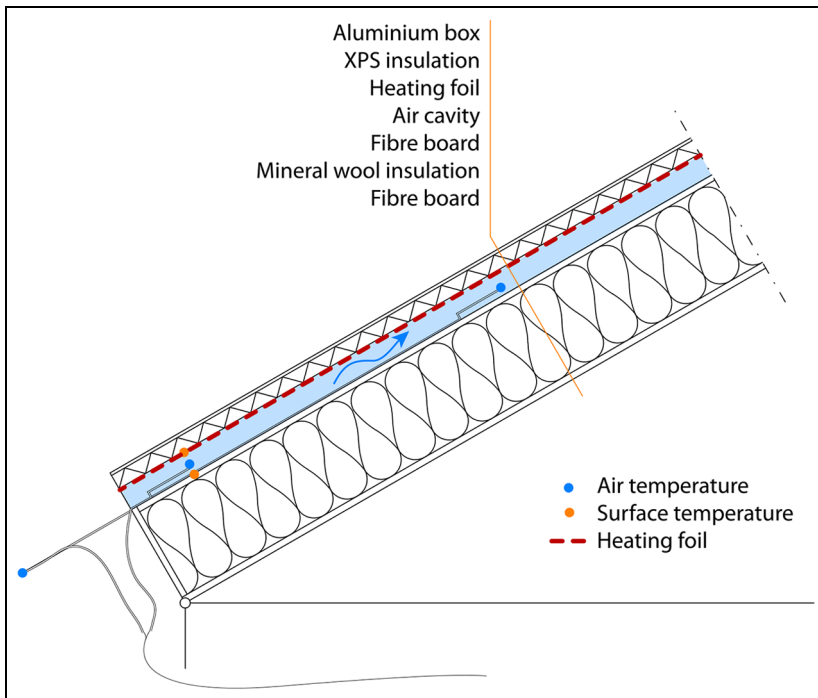


Figure 6. Schematic view of the experimental setup. The dots represent measuring points for air and surface temperature. The cavity had a length of 3500 mm, and a width of 500 mm. Full information on the experimental setup is provided in Svantesson and Säwén (2019).

Comparative studies

As a basis for assessment of the output of the Thermal Buoyancy Model, two comparative studies were performed. Firstly, an experimental study was conducted, and secondly, numerical simulations were performed. Finally, the Thermal Buoyancy Model was implemented using MATLAB to allow for comparison.

Experimental study

The experimental study was performed at one of the laboratories of SINTEF and NTNU in Trondheim, Norway (Bunkholt, 2019; Bunkholt et al., 2020; Svantesson and Säwén, 2019). Experiments were conducted on a full-scale model of a section of a cavity-ventilated roof construction, represented schematically in Figure 6. The model was built by Gullbrekken (2018), and modified for this study. In the model, the roof inclination and air cavity height could be changed to study different geometrical configurations of the air cavity and their effect on the thermal buoyancy.

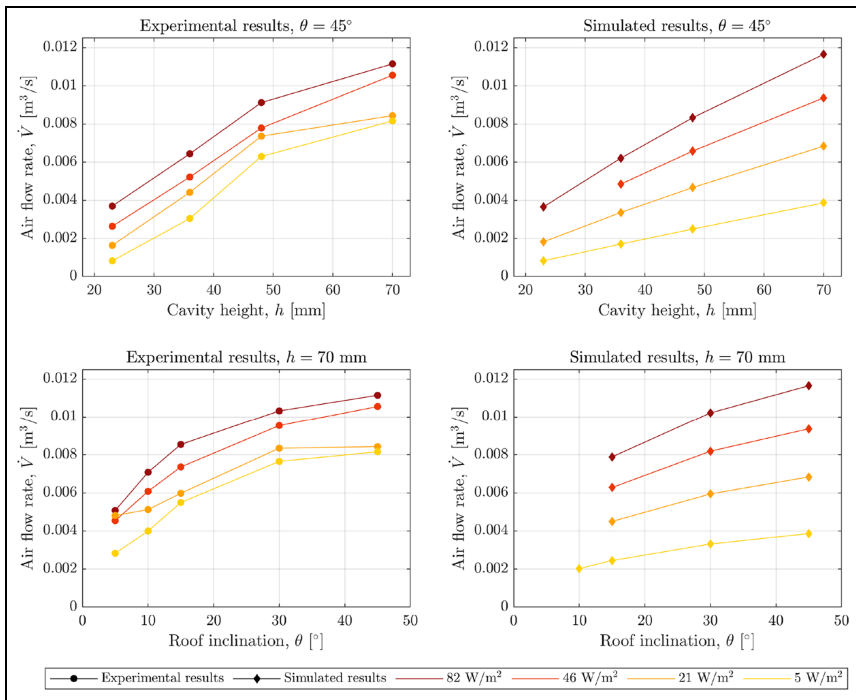


Figure 7. Air flow rate \dot{V} as a function of air cavity height h and roof inclination θ in the experimental and numerical studies, for two of the cases studied. In the first case the roof inclination is fixed at $\theta = 45^\circ$. In the second case, the air cavity height is fixed at $h = 70$ mm. The differently coloured lines represent different heat intensities I applied to the heating foil. Note that some of the data points in the numerical study are missing due to divergence of the numerical model.

Heat was introduced using a heating foil along the top inner surface of the air cavity to simulate solar radiation on a roof surface.

Tests were performed for roof inclinations between 5 and 45° , and for cavity heights between 23 and 70 mm, corresponding to typical Nordic roof designs. The length of the test roof was 3500 mm, and the width of the cavity 500 mm. The effective heat transfer coefficient α_0 for the roof calculated according to the process outlined in Figure 3 was $\alpha_0 \text{ W}/(\text{m}^2 \cdot \text{K})$ under the studied thermal conditions (Svantesson and Sävén, 2019).

The heat loads applied through the heating foil mounted inside the cavity ranged between 5 and $80 \text{ W}/\text{m}^2$. Considering roof surface absorptivity and heat transmission, this was estimated to correspond to solar heat intensities of 100–1000 W/m^2 on a real construction with solar absorptivity $\alpha_{sol} = 0.94 \text{ W}/(\text{m}^2 \cdot \text{K})$. This estimation was done using similar techniques of network analysis as showcased in

Figure 3. Various roof inclinations, air cavity heights, and applied heat loads were combined in 80 different test set-ups. For each test set-up, the surface and air temperatures were measured using thermocouples attached to the model. The air flow rate was estimated using smoke tests. Smoke was released from a smoke-pen or a sampling tube, and the time was measured for the smoke to travel through the cavity. Five measurements were performed for each case, and the average value was assumed to correspond to the maximum velocity of the air flowing through the cavity (Svantesson and Säwén, 2019). The coefficient of variation for these tests was in the range of 2%–10%.

Numerical study

The numerical study was performed using the CFD module of COMSOL Multiphysics (COMSOL, 2017). To simulate air flow due to thermal buoyancy, the non-isothermal flow physics module was selected (Svantesson and Säwén, 2019).

To reduce computational cost, the cavity was modelled in two dimensions with no influence of the cavity edges on the air flow rate. The cavity was represented in the Finite Element Model using a free triangular mesh, with a quad mesh representing the cavity boundary layer. A maximum element size of 0.01 m was selected.

The same test set-ups were simulated as in the experimental study, with roof inclinations between 5° and 45°, and for cavity heights between 23 and 70 mm. The cavity length was 3500 mm. Based on early estimates for Reynolds numbers, laminar flow conditions were assumed. This assumption was later shown to hold for most test cases, as seen in Figure 9. The heat applied to the heating foil in the experimental model was represented by a convective heat flux along the cavity top surface, with heat fluxes of ((5 W/m² – 80 W/m²).

Out of 80 test set-ups considered in the parametric sweep, 58 achieved convergence. Some of the divergent configurations were modified to improve convergence, with limited success, likely due to numerical issues with the boundary conditions (Svantesson and Säwén, 2019).

Implementation of Thermal Buoyancy Model

The analytical Thermal Buoyancy Model has been implemented in MATLAB and is available as an Open Source project (Stockhaus and Säwén, 2020). As every given roof construction exists in different conditions, there may be a need for modifications, for example to the calculation of the effective heat transfer coefficient α_0 , to obtain representative results. Of note is that the model considers steady-state conditions, which may not be realistic for rapid changes in solar heat load. Also, the model is not applicable when the wind is the governing driving force for the air cavity flow.

To allow for comparison, the same test set-ups as in the experimental and numerical studies were modelled using the Thermal Buoyancy Model. For each test set-up, the following parameters are inputs to the model:

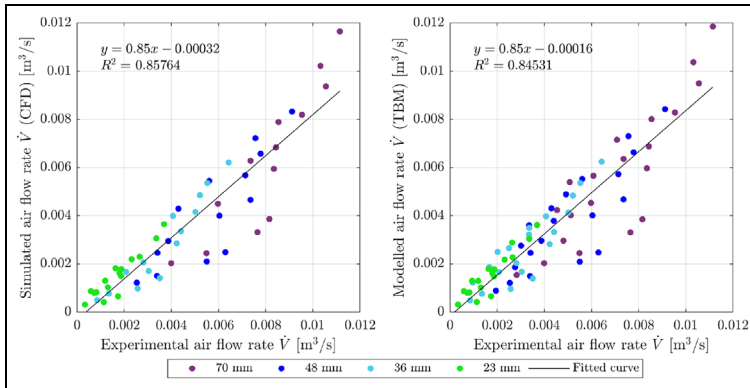


Figure 8. Air flow rate \dot{V} in the experimental study in comparison with the numerical study (CFD) and the Thermal Buoyancy Model results (TBM) respectively, for all set-ups, with the differently coloured dots representing different cavity heights.

- Ambient air temperature T_e [K]
- Effective air temperature T_0 [K]
- Effective heat transfer coefficient α_0 [W/(m² K)]
- Relative humidity RH [%]
- Cavity inclination θ [°]
- Cavity width b [m]
- Cavity height h [m]

These parameters could all be used as defined or calculated in the comparative studies. Specifically, T_0 and α_0 for each test set-up were calculated according to the steps outlined in Figure 3.

Analysis and comparison

For the experimental and numerical studies, quantitative results were obtained for the air flow and thermal conditions in the air cavity.

The results of the simulations were found to correspond well to the experimental results, as seen in Figure 7, which shows measured and simulated air flow rates through the air cavity for some of the test set-ups. The trends are similar. As expected, an increased heat load or roof inclination caused an increased air flow rate, due to an increased driving force. An increased cavity height resulted in an increased air flow rate due to a decreased air flow resistance.

Using the known cavity geometry, the driving force and air flow resistance could then be calculated, allowing a comparison with the analytical Thermal Buoyancy Model. The full results of the comparative studies, compared with the output of the Thermal Buoyancy Model, can be seen in Figure 8.

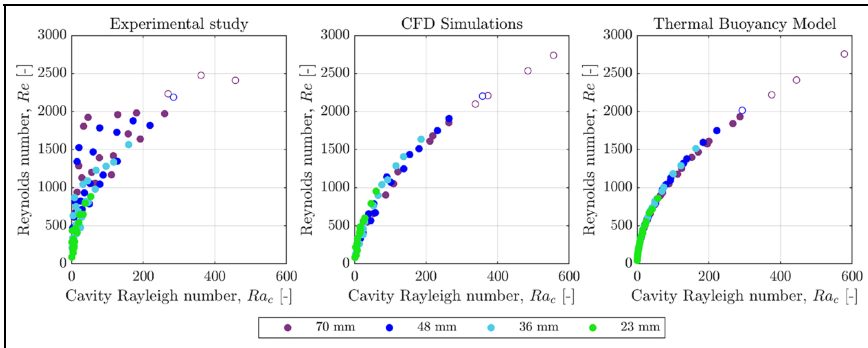


Figure 9. Reynolds number Re , as calculated from the air flow rate \dot{V} measured in the experimental study, simulated in the numerical study, and predicted by the Thermal Buoyancy Model, respectively. The differently coloured dots represent different air cavity heights. Hollow dots exceeded the critical Reynolds number $Re_{crit} = 2000$, and have been excluded from the statistical analysis.

The calculated cavity Rayleigh number, Ra_c , for each test set-up in the experimental and numerical studies is plotted against the Reynolds number, Re , calculated from the measured/simulated/predicted air flow rate, \dot{V} , in Figure 9. The relationship is clear to be seen in all three studies. For most cases, the assumption of laminar flow was found to hold, that is $Re < Re_{crit} = 2000$. The cases where the critical Reynolds number was exceeded have been excluded from the statistical analysis.

Performing a curve fit using a single term power series model on the values provides the result shown in Figure 10. The experimental study generally estimates higher air flow rates than the numerical and analytical studies. On average, in the relevant regime where $Re < Re_{crit} = 2000$, the experimental study shows a 29% higher air flow rate than predicted by the simulations, and a 24% higher air flow rate compared to the Thermal Buoyancy Model prediction. In turn, the Thermal Buoyancy Model predicts a 3% higher air flow rate, on average, than the numerical study.

The difference in the results can be explained largely by the simplifications and assumptions made when setting up the different models. For instance, any imperfections and measurement uncertainties in the experimental model will have a stronger impact for lower air flow rates, which were notably more difficult to measure confidently. The simulations also include a number of simplifications (mesh size, 2D approximation, etc.) in order to achieve convergence in a reasonable time frame. Nevertheless, based on the comparative studies, the correspondence is strong enough that the Thermal Buoyancy Model can be regarded as a useful tool and as an efficient complement to time-consuming CFD simulations.

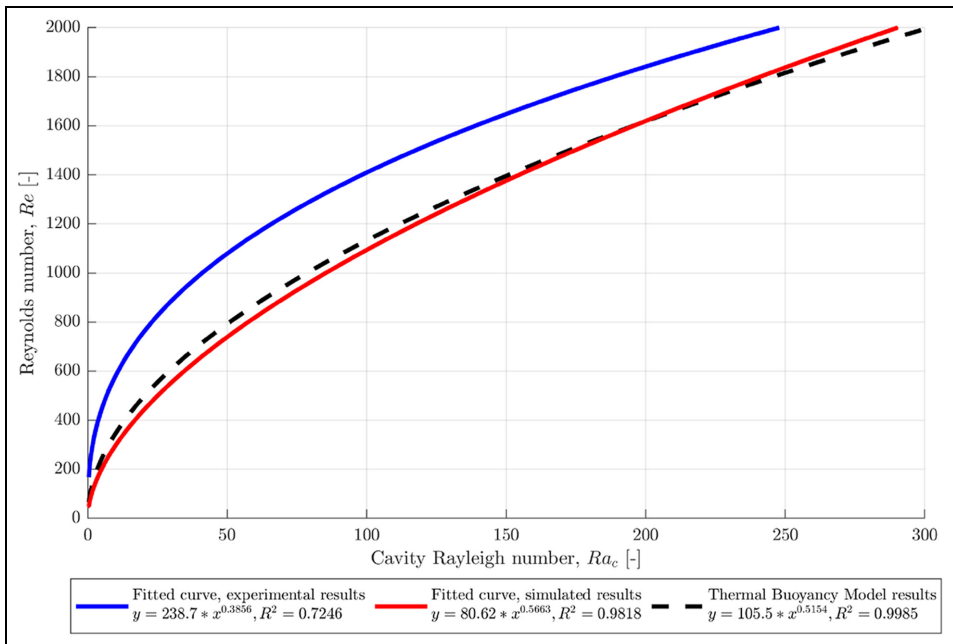


Figure 10. Reynolds number Re as calculated from the air flow rate \dot{V} measured in the experimental study, simulated in the numerical study, and predicted by the Thermal Buoyancy Model, respectively. Curve fits performed using a single term power series model, excluding values which exceeded the critical Reynolds number $Re_{crit} = 2000$.

Application: Case study

To evaluate the relevance of thermal buoyancy in the context of natural roof cavity ventilation, the driving force due to thermal buoyancy calculated using the Thermal Buoyancy Model was compared to the driving force of wind (Svantesson and Säwén, 2019). The thermal driving force for typical weather cases was found to be comparable in magnitude to the driving force of wind with a speed of 1 m/s or less perpendicular to the ventilation openings. In the studied climate, such conditions where thermal buoyancy is of relevance arise for over 25% of the year, meaning that the thermally induced air flow could be of great relevance to the drying potential of the air cavity. Indeed, as noted by Vanpachtenbeke et al. (2017), sunny days with little wind are of greater importance to the drying process than cloudy, windy days.

The model was applied in a case study performed on a reference roof construction shown in Figure 1. The construction was chosen for being a typical design in Nordic climates as well as for its inherent moisture safety problems. Based on the roof materials, the roof construction has a calculated $\alpha_0 = 2.29 \text{ W}/(\text{m}^2 \cdot \text{K})$. The

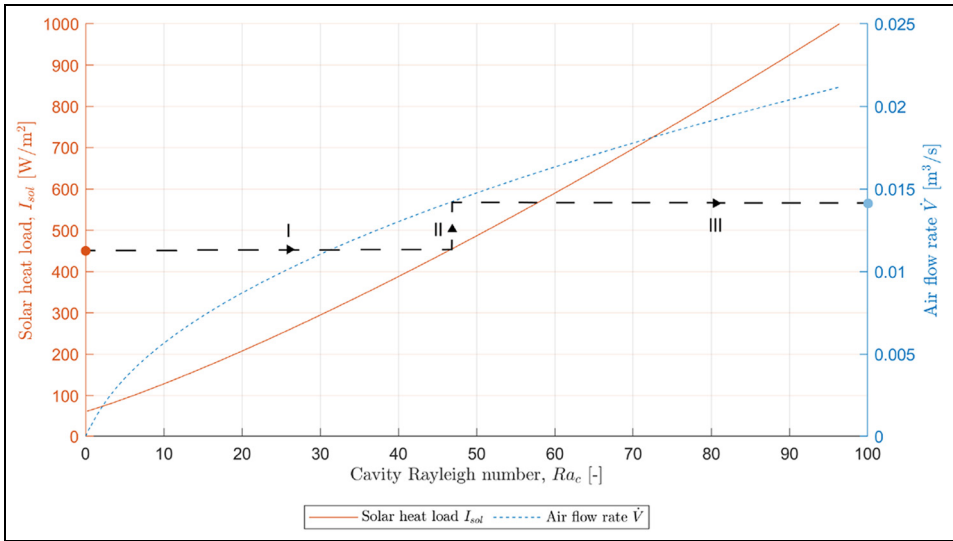


Figure 11. Example output and usage of the Thermal Buoyancy Model. This graph shows the relationship between I_{sol} , Ra_c and \dot{V} in the case study construction with $\alpha_0 = 2.29 \cdot \text{W}/(\text{m}^2 \cdot \text{K})$, and for a specific $T_e = 20^\circ\text{C}$. For a given solar heat load $I_{sol} = 450 \text{ W}/(\text{m}^2 \cdot \text{K})$, (I) provides the calculated cavity Rayleigh number, and (II) and (III) allows for a prediction of the air flow rate, $\dot{V} = 14.1 \cdot 10^{-3} \text{ m}^3/\text{s}$.

air cavity width in the roof is 0.552 m, the roof length from inlet to outlet is 10 m, the cavity height is 0.045 m, and the inclination is 30° .

The values calculated by the Thermal Buoyancy Model when applied in the case study are displayed in Figure 11. Here, the cavity Rayleigh number is calculated as a function of the solar heat load, represented by the orange line. Then, the air flow rate is calculated based on the cavity Rayleigh number, as represented by the dotted blue line. Thus, for any given climate conditions, the air flow rate can be predicted. As an example, for a given solar heat load $I_{sol} = 450 \text{ W}/(\text{m}^2 \cdot \text{K})$, line (I) provides the calculated cavity Rayleigh number, and lines (II) and (III) allows for a prediction of the air flow rate, $\dot{V} = 14.1 \cdot 10^{-3} \text{ m}^3/\text{s}$.

Note that the graph shown in Figure 11 will look different for any given construction and for different climate conditions, as the effective heat transfer coefficient α_0 , as well as the outdoor air temperature T_e , affect the relationship between solar heat load, cavity Rayleigh number and air flow rate.

Conclusion

In the present study, a novel analytical model, called the Thermal Buoyancy Model, was devised to predict the air flow rate in a cavity-ventilated roof

construction, by means of calculating the cavity Rayleigh number for the present climatic conditions and design of the air cavity. The cavity Rayleigh number is a dimensionless representation of the driving force, flow resistance and thermal properties of the fluid and roof materials. Its relationship with the characteristic length for heating of the flowing air allows predicting the thermal conditions in the air cavity, and by extension calculation of the air flow rate.

The Thermal Buoyancy Model output was compared to the results of an experimental and a numerical study, where the flow behaviour in typical roof constructions was investigated. On average, the predicted air flow rate was found to be underestimated by 20% in comparison with the experimental study, and overestimated by 3% compared to the numerical study. However, the trends were similar in both the Thermal Buoyancy Model output and the two comparative studies.

The Thermal Buoyancy Model can be applied in the evaluation of the performance of a roof construction, by using the predicted air flow rate as an input for hygrothermal simulations.

In future research, the impact of wind on the thermal conditions and the flow driving forces could be included to expand the model and allow its application in assessing the moisture safety or thermal efficiency of cavity-ventilated roof constructions.

Acknowledgement

The authors would like to thank Tore Kvande, NTNU, and Lars Gullbrekken, SINTEF, for their support in the experimental study. The authors would also like to thank Kaj Pettersson and Fredrik Domhagen, Chalmers University of Technology, for support in the numerical study and for valuable input, and to thank Staffan Sävén for editing assistance.


Declaration of conflicting interests

The author(s) declared no potential conflicts of interest with respect to the research, authorship, and/or publication of this article.

Funding

The author(s) received no financial support for the research, authorship, and/or publication of this article.

ORCID iD

Toivo Sävén  <https://orcid.org/0000-0001-7989-3021>

References

Arvidsson J, Harderup LE and Samuelson I (2017) *Fukthandbok: praktik och teori*, 4th edn. Stockholm: AB Svensk Byggtjänst.

- Biwole PH, Woloszyn M and Pompeo C (2008) Heat transfers in a double-skin roof ventilated by natural convection in summer time. *Energy and Buildings* 40(8): 1487–1497.
- Blom P (1991) *Lufting av isolerte, skrå tak*. Doctoral dissertation, NTH, Trondheim.
- Blom P (2001) Venting of attics and pitched, insulated roofs. *Journal of Thermal Envelope and Building Science* 25(1): 32–50. DOI: 10.1106/9HUC-8X0C-Y34R-RAGW.
- Bunkholt NS (2019) *Eksperimentell studie av termisk oppdrift i tak med luftet tekning*. Master's thesis, NTNU, Trondheim.
- Bunkholt N, Säwén T, Stockhaus M, et al. (2020) Experimental study of thermal buoyancy in the cavity of ventilated roofs. *Buildings* 10: 8. DOI: 10.3390/buildings10010008.
- Bunnag T, Khedari J, Hirunlabh J, et al. (2004) Experimental investigation of free convection in an open-ended inclined rectangular channel heated from the top. *International Journal of Ambient Energy* 25(3): 151–162.
- Chami N and Zoughaib A (2010) Modeling natural convection in a pitched thermosyphon system in building roofs and experimental validation using particle image velocimetry. *Energy and Buildings* 42(8): 1267–1274.
- COMSOL (2017) *Introduction to COMSOL Multiphysics*. COMSOL.
- DeWith G, Cherry N and Haig J (2009) Thermal benefits of tiled roofs with above-sheathing ventilation. *Journal of Building Physics* 33(2): 171–194.
- Falk J (2014) *Rendered rainscreen walls cavity ventilation rates, ventilation drying and moisture-induced cladding deformation*. Doctoral dissertation. Lund University, Sweden.
- Griffith B (2006) Model for naturally ventilated cavities on the exteriors of opaque building thermal envelopes. Technical report. National Renewable Energy Lab. (NREL), Golden, CO.
- Gullbrekken L (2018) *Climate adaptation of pitched wooden roofs*. Doctoral thesis, NTNU, Trondheim.
- Hagentoft CE (1991) Air convection coupled with heat conduction in a wall. A thermal analysis. *Notes on Heat Transfer* 7.
- Hagentoft CE (2001) *Introduction to Building Physics*. Lund: Studentlitteratur AB.
- Hansen H, Stampe O and Kjerulf-Jensen P (1992) *Varme og klimateknik: grundbog*. Glostrup: DANVAK.
- Kronvall J (1980) *Air flows in building components*. Doctoral dissertation, Lund University, Sweden.
- Lee S, Park SH, Yeo MS, et al. (2009) An experimental study on airflow in the cavity of a ventilated roof. *Building and Environment* 44(7): 1431–1439.
- Li D, Zheng Y, Liu C, et al. (2016) Numerical analysis on thermal performance of naturally ventilated roofs with different influencing parameters. *Sustainable Cities and Society* 22: 86–93. Available at: <http://www.sciencedirect.com/science/article/pii/S2210670716300178> (accessed 4 January 2021).
- Liersch KW (1986) *Belüftete Dach- und Wandkonstruktionen, Band 3: Dächer*. Berlin: Bauverlag.
- Manca O, Mangiacapra A, Marino S, et al. (2014) Numerical investigation on thermal behaviors of an inclined ventilated roof. In: *Dynamics, Vibration and Control; Energy; Fluids Engineering; Micro and Nano Manufacturing*, vol. 2. ASME, V002T09A017.
- MATLAB (2020). *vpasolve*. Available at: <https://www.mathworks.com/help/symbolic/vpasolve.html> (accessed 2 July 2020).
- Nore K, Blocken B and Thue J (2010) On CFD simulation of wind-induced airflow in narrow ventilated facade cavities: Coupled and decoupled simulations and modelling limitations. *Building and Environment* 45(8): 1834–1846.

- Petersson BA (2009) *Byggnaders klimatskärm: fuktsäkerhet, energieffektivitet, beständighet*. Sweden, Lund: Studentlitteratur.
- SMHI (2019) *Utforskaren - Öppna data*. Available at: <https://www.smhi.se/data/utforskaren-oppna-data> (accessed 4 January 2021).
- Stockhaus M and Säwén T (2020) *Thermal buoyancy model*. <https://github.com/sawenchalmers/thermal-buoyancy-model> (accessed 4 January 2021).
- Susanti L, Homma H, Matsumoto H, et al. (2008) A laboratory experiment on natural ventilation through a roof cavity for reduction of solar heat gain. *Energy and Buildings* 40(12): 2196–2206.
- Svantesson M and Säwén T (2019) *Ventilation by thermal buoyancy in the air cavity of pitched wooden roofs*. Master's thesis, Chalmers University of Technology, Gothenburg. Available at: <https://hdl.handle.net/20.500.12380/300084> (accessed 4 January 2021).
- Tieben J, Bachinger J and Nusser B (2020) Development of a statistical model to assess the climate conditions in the ventilation layer of double pitched roofs. In: *E3S Web of Conferences. Proceedings of the 12th Nordic Symposium on Building Physics (NSB 2020)*, vol. 172, p. 11005. EDP Sciences.
- Van Belleghem M, Steeman M, Janssens A, et al. (2015) Heat, air and moisture transport modelling in ventilated cavity walls. *Journal of Building Physics* 38(4): 317–349. DOI: 10.1177/1744259114543984.
- Vanpachtenbeke M, Langmans J, Van den Bulcke J, et al. (2017) On the drying potential of cavity ventilation behind brick veneer cladding: A detailed field study. *Building and Environment* 123: 133–145.
- Viljanen K, Lü X and Puttonen J (2020) Hygrothermal behaviour of ventilation cavities in highly insulated envelopes. In: *E3S Web of Conferences. Proceedings of the 12th Nordic Symposium on Building Physics (NSB 2020)*, vol. 172, p. 07003. EDP Sciences.